In: Wagner W., Székely, B. (eds.): ISPRS TC VII Symposium – 100 Years ISPRS, Vienna, Austria, July 5–7, 2010, IAPRS, Vol. XXXVIII, Part 7B

Contents   Author Index   Keyword Index

RECOGNITION OF WINDING DISPLACEMENTS FOR STEEL COILS VIA LASER LIGHT SECTION TECHNIQUE

Patrick A. Hölzl, Daniel C. H. Schleicher and Bernhard G. Zagar

Johannes Kepler University
Institute for Measurement Technology
Austria, Linz 4040
patrick.hoelzl@students.jku.at, daniel.schleicher@jku.at, bernhard.zagar@jku.at

KEY WORDS: Laser scanning, Measurement, Three–dimensional, Object, Pattern, Recognition, Segmentation, Industrial

ABSTRACT:

To satisfy the ever increasing quality standards of todays steel industry the basic products, in this case steel coils, must be produced within very small tolerances. To achive those quality limits, control systems via machine vision are getting more and more popular. For example the quality level of steel coils decreases due to winding displacements based on a non–ideal production process. In this paper a machine vision system for the recognition of winding displacements of steel coils, based on the laser light sectioning technique, will be presented. The introduction of the mathematical model of the laser light sectioning setup allows to compensate some influences of the setups inaccuracies. We show that a reliable recognition of the coil profile with an accuracy below or less than 1mm can be achieved by a rather simple adaptive algorithm. Finally defects can be detected accurately out of the recognized coil profile.

1 INTRODUCTION

Generally metal processing companies, like car manufacturer get their basic material in form of rolled up steel sheets, called coils. These metal processing companies and especially the steel industry are interested in systems to detect defects and to minimize material rejects. One of the major problems which can occur durring the coil manufactoring process are displacements of windings, due to a non–conform rolling–up process or a faulty packaging. These winding displacements cause a higher percentage of non usable material and so for quality aspects a preventive detection of these displacements is necessary. Figure 1 shows a model of the coil and winding displacements. The winding displacements $h(r)$ typically are less than 5 mm, larger displacements are problematic and are aimed to be detected by our system. To achieve this requirement for the profil resolution the minimum detectable winding displacement $h_{min}(r)$ is specified to be equal to or less than 1 mm.
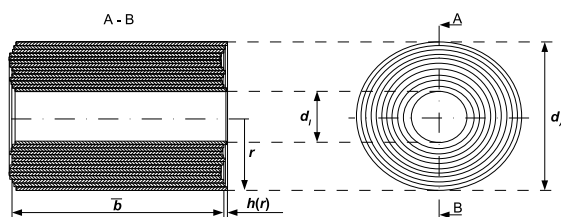
Figure 1: Model of the coil with winding displacements $h(r)$ indicated, d_i and d_a are the inner and outer diameter of the coil respectively and $\bar{b}$ is the mean coil width.

For the above–mentioned model we imply three assumptions which are realistic for further processing:

1. An axial winding displacement $h(r)$ on one side results in an inverse displacement $-h(r)$ on the other side (implying $\bar{b}$ is constant for each winding).

2. The winding displacement $h(r)$ is constant over one winding at radius r.

3. Winding displacements along the radius r occurs only in small steps.

Due to the first assumption we only need to look for defects on one cylinder base. The second assumption limits the ROI to one radial range of zero to $d_A/2$ thus improving resolution. So for the further recognition process the ROI will be limited to the lower half of the coil as indicated in Fig. 2 (red rectangle). The last assumption is necessary for the recognition algorithm presented in Sec. 4 to work correctly. The complete detection should happen during the coils storage process, that means the coil will move during the measurement. Figure 2 shows a typical storing process, with the coil on a transport waggon moving in axial direction with 0.5 m/s. The problem here is that the storage process can not be influenced or changed, so the chosen measurement method must be adapted to these conditions. Therfore an optical 3D measurement method is the best choice with respect to cost and resolution. Due to the varying lighting conditions in the storage facility, which can not be influenced, the realized measurement system and furthermore the machine vision system must be very robust with respect to natural illumination conditions.

Figure 2: Moving steel coil on transport waggon during the storing process, with a blurred laser line barely visible in the ROI (red rectangle).

Considering the given terms a detection system based on the laser light sectioning technique (Kraus, 1996, Wu et al., 1993) is the preferred choice. Figure 3 shows the principle behind the laser light section technique. The elevation profile of interest is illuminated from an off-center position by a line shaped laser light fan. So the lateral displacement $d(r)$ of the projected line as viewed at from a vantage point orthogonal to the front side of the measure-

In: Wagner W., Székely, B. (eds.): ISPRS TC VII Symposium – 100 Years ISPRS, Vienna, Austria, July 5–7, 2010, IAPRS, Vol. XXXVIII, Part 7B

Contents | Author Index | Keyword Index

ment probe (see Fig. 4) is a scaled replica of the profile height $h(r)$.
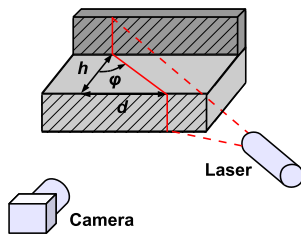
Figure 3: Scheme for the laser light section technique with the geometric triangle drawn in produced by the line shaped light source.

$$\frac{d(r)}{h(r)} = \tan(\varphi) \quad (1)$$

$$h(r) = \frac{d(r)}{\tan(\varphi)} \quad (2)$$
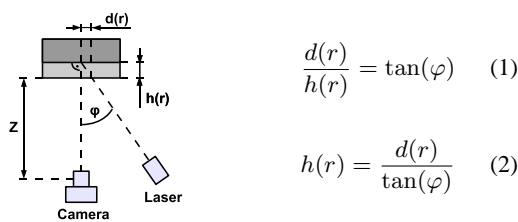
Figure 4: Top view from the laser light section technique scheme.

The smallest clearly recognizable profile height depends on the triangulation angle, φ, which is measured between the incidence direction of the light source and the surveying direction of the camera and the pixel pitch. For optical reasons (reflection properties of the coil) and resolution considerations the triangulation angle φ should be between $30°$ and $60°$ (Schäfter and Kirchhoff, 2004).

To minimize the influence of the varying lighting conditions a powerful diode laser with 100 mW at 660 nm is used as light source and additionally an optical bandpass filter is used to reduce the ambient lights influence. The optical bandpass (see Fig. 5) consists of two separate filters, a near infrared blocking filter and a red filter. The combination of both filters results in an optical bandpass with a maximum transmission of 94 % at a central wavelength (CWL) of 685 nm and a full width at half maximum (FWHM) bandwidth of 100 nm. Compared to a standard interference filter the assembled optical bandpass has a larger FWHM bandwidth but shows no dependency on the angle of incidence, which is known to cause spectral side effects for interference filters.
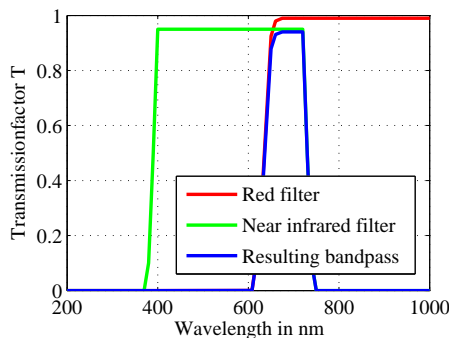
Figure 5: Diagramm of the filter transmittance, the near infrared blocking filter (green), the red filter (red) and the resulting optical bandpass (blue).

The second possibility to minimize the influence of the lighting conditions is to reduce the shutter time. This is also necessary with regard to the movement of the coil during the measurement.

2 EXPERIMENTAL SETUP

Before a recognition system based on the laser light sectioning technique is realized, the camera characteristics and furthermore the depth resolution limits have to be determined. First of all an approximation of the minimum detectable object size is necessary, therefore the specifications of the provided camera and the expected viewing geometry must be known:

- Pixel pitch p: 4.65 μm
- Focal length f: 30 mm (camera constant $c \approx f$)
- Distance between camera and coil Z: 5 m

By using Eqn. 3, which describes the central projection theorem (Luhmann, 2003) (with the object dimensions in real world x and on the CCD chip x'), we obtain a minimum detectable object size x_{min} of 0.7486 mm.

$$x' = \frac{x}{\frac{Z}{c} + 1} \quad \rightarrow \quad x_{min} = p\left(\frac{Z}{c} + 1\right) \quad (3)$$

The minimum detectable object size x_{min} can now be used to designate the triangulation angle φ (in Eqn. 2). In Fig. 6 the relationship between φ and the minimum detectable winding displacement h_{min} is plotted.
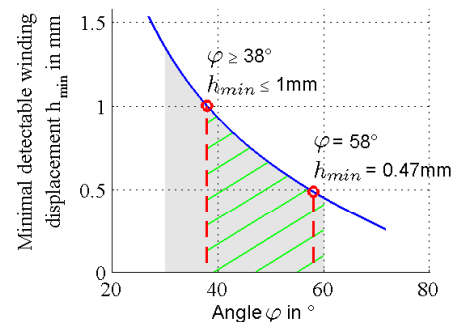
Figure 6: Relationship between φ and the minimum detectable winding displacement h_{min}. The required and realized operating points for the minimum detectable winding displacement h_{min} are marked with red dashed lines. The gray colored area indicates the interval of technically relevant triangulation angles φ. The green hatched area labels the interval of valid triangulation angles φ for the realization.

The minimum detectable winding displacement h_{min} was specified to be equal to or less than 1mm. Therefore the triangulation angle φ is choosen to be $58°$, and the resulting minimum detectable winding displacement h_{min} is 0.47 mm. Due to the measurement error which will be calculated in Sec. 5 a value less than 1mm is advantageous. A major requirement for using the laser light section technique is the presence of a diffusely reflecting object. This can be proved with the Rayleigh criterion (Horbach, 2008) shown in Eqn. 4.

$$R_a < \frac{\lambda}{16\cos(\varphi)} \quad (4)$$

The Rayleigh criterion is an inequation including the wavelength of light λ, the triangulation angle φ and the mean roughness index R_a. If the mean roughness index R_a of the illuminated object area is less than $\lambda/16\cos(\varphi)$ no diffuse reflection appears

In: Wagner W., Székely, B. (eds.): ISPRS TC VII Symposium – 100 Years ISPRS, Vienna, Austria, July 5–7, 2010, IAPRS, Vol. XXXVIII, Part 7B

Contents   Author Index   Keyword Index

according to this law. By evaluating the inequation it follows that a diffuse reflection appears if $R_a \geq 77.842$ nm. The mean roughness index R_a of the coil front surface is between 6 μm and 11 μm and therefore it is sufficient to guarantee diffuse reflection.

To proof the assumptions made in this section an experimental setup has been designed. The coil windings are modelled by several steelplates of the same thickness which are stacked upon each other and then deferred fixed. First a frontal photograph of the coil winding model including the laser line was taken to calculate the displacements with the laser light section technique, shown in Fig. 7(a). Because of the good illumition conditions only an optical red filter was used. Additionally a photograph from the side was taken as reference image for the coil winding model, shown in Fig. 7(b).
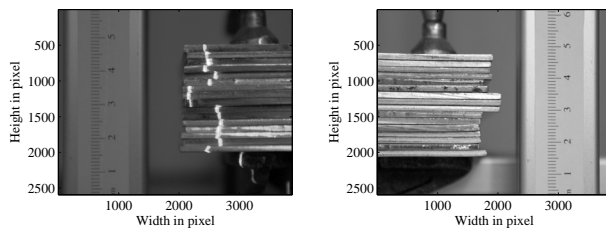
(a) Frontal photograph of the coil winding model showing the laser line.

(b) Lateral photograph of the coil winding model.

Figure 7: Photographs of the coil winding model.

To determine the winding displacement, the first step is to extract the laser line from the acquired image data. Therefore the image is cropped to the probe edges and then the position of maximum intensity in every row is determined. For the experimental setup a commercial photo camera was used, whos images were downsampled to obtain a comparable resolution to typical video cameras. The reference for the coil winding model is obtained from the lateral image by using a canny edge detection algorithm (Gonzalez and Woods, 2008). In Fig. 8 the results of the previous steps are shown. The laser light section curve is close to the reference curve and also the desired resolution limit is almost reached.
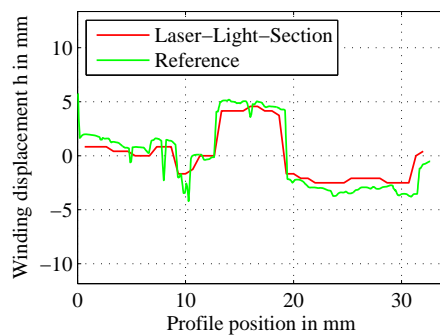
Figure 8: The red colored curve is the result for the displacement recognition by using the laser light section technique and the green colored curve is the reference derived from the frontal probe image (see Fig. 7(a)). A good agreement can be seen.

3   ADVANCED MODELING OF THE SETUP

During the experimental setup the influence of the laser alignment on the result was very low because of the small–sized probe with a height of only 32 mm (a typical coil profile length can be up to 700 mm). Considering a profile length of 700 mm a slight rotation of the laser around its symmetry axis by 0.3°, re-

sults in a maximum error of 6 mm for the displacement determination. Futhermore the coil windings can also be affected by a linear trend due to a non–conform rolling–up process. This linear trend can be used as a quality characteristic too and should therefore also be measured. To estimate the influence of the laser alignment and the linear trend of the coil front on the laser line a model of the setup is introduced in Fig. 9. Here two coordinate systems are considered, a fixed–place coordinate system given by x, y, z and a laser coordinate system given by ξ, η, ζ. The laser coordinate system is rotated by the angles α, β, γ which allow a free rotation of the laser in space with the corresponding rotation matrices (Cook, 2007) shown in Eqns. 5, 6 and 7. For a solvable system of equations it is necessary to pose the following constraint on the coil windings and the laser line. The additional linear trend resulting from the non–conform rolling–up processes is represented by a rotation of the coil front around the y–axis by an angle θ with the corresponding rotation matrix shown in Eqn. 8. That means that when the laser line is projected onto the axis of symmetry in the lower half of the coil only a linear trend is present in the x–direction. This can be achieved by an exact triggering and a limitation on the ROI.
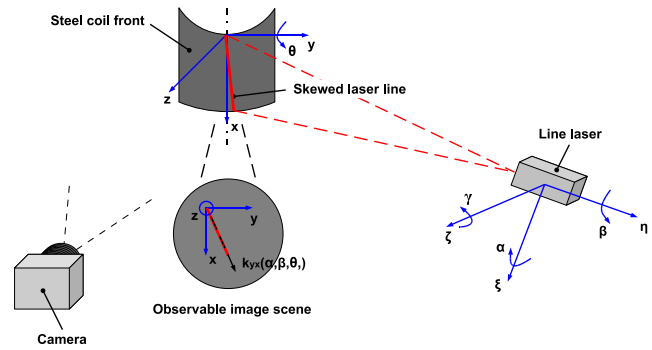
Figure 9: Advanced model of the setup with a fixed–place coordinate system given by x, y, z and a laser coordinate system given by ξ, η, ζ.

The following rotation matrices R_γ, R_β, R_α and R_θ represent the degrees of freedom in the setup:

- Rotation around ζ, for up or down tilting of the laser.

$$\underline{R}_\gamma = \begin{pmatrix} \cos(\gamma) & -\sin(\gamma) & 0 \\ \sin(\gamma) & \cos(\gamma) & 0 \\ 0 & 0 & 1 \end{pmatrix} \qquad (5)$$

- Rotation around η, for rotation of the laser around its symmetry axis.

$$\underline{R}_\beta = \begin{pmatrix} \cos(\beta) & 0 & \sin(\beta) \\ 0 & 1 & 0 \\ -\sin(\beta) & 0 & \cos(\beta) \end{pmatrix} \qquad (6)$$

- Rotation around ξ, for tangential deviation of the laser due to the laser light section technique in the following form $\alpha = \varphi - \pi/2$.

$$\underline{R}_\alpha = \begin{pmatrix} 1 & 0 & 0 \\ 0 & \cos(\alpha) & \sin(\alpha) \\ 0 & -\sin(\alpha) & \cos(\alpha) \end{pmatrix} \qquad (7)$$

- Rotation around y, for skewness of the coil front.

$$\underline{R}_\theta = \begin{pmatrix} \cos(\theta) & 0 & \sin(\theta) \\ 0 & 1 & 0 \\ -\sin(\theta) & 0 & \cos(\theta) \end{pmatrix} \qquad (8)$$

With the given rotation matrices the normal vector for the coil front $\vec{v}_{Cn}$ and the normal vector for the triangular shaped area spanned by the laser $\vec{v}_{Ln}$ can be calculated in the fixed–place coordinate system, shown in Eqns 9 and 10.

$$\vec{v}_{Ln} = \underline{R}_\alpha \cdot \underline{R}_\beta \cdot \underline{R}_\gamma \cdot \underbrace{\begin{pmatrix} 0 \\ 0 \\ 1 \end{pmatrix}}_{\vec{e}_\zeta} = \begin{pmatrix} \sin(\beta) \\ \sin(\alpha)\cos(\beta) \\ \cos(\alpha)\cos(\beta) \end{pmatrix} \quad (9)$$

$$\vec{v}_{Cn} = \underline{R}_\theta \cdot \underbrace{\begin{pmatrix} 0 \\ 0 \\ 1 \end{pmatrix}}_{\vec{e}_{Coil}} = \begin{pmatrix} \sin(\theta) \\ 0 \\ \cos(\theta) \end{pmatrix} \quad (10)$$

Then the direction of the intersection vector $\vec{u}$ between the coil front and the laser can be determined by the cartesian product of the according normal vectors $\vec{v}_{Cn}$ and $\vec{v}_{Ln}$, shown in Eqn. 11. Now the intersection of the coil front and the triangular shaped area spanned by the laser, results in the visible laser line on the coil with the coordinates (x_L, y_L, z_L). The intersection vector $\vec{u}$ is a scaled version (by a factor ν) of the laser line with the same orientation, see Eqn. 12. Further the intersection vector $\vec{u}$ is independent of γ so the orientation of the laser line is independent of an up or down tilting of the laser.

$$\vec{u} = \vec{v}_{Ln} \times \vec{v}_{Cn} \quad (11)$$

$$\begin{pmatrix} x_L \\ y_L \\ z_L \end{pmatrix} = \nu \, \vec{u} \quad (12)$$

To eliminate the influence of the laser alignment and the linear trend of the coil front the remaining angles β and θ must be calculated. Therefore the orientation of the laser line will be separatlly examined in the y,x–plane and in the y,z–plane. Due to the setup the orientation of the laser line k_{yx} in the y,x–plane is present in the observable image scene in Fig. 9 and can be measured by a trend estimation of the extracted laser line, the associated relation of the laser coordinates y_L and x_L is shown in Eqn. 13.

$$k_{yx} = \frac{y_L}{x_L} = \frac{\cos(\alpha)\cos(\beta)\sin(\theta) - \sin(\beta)\cos(\theta)}{\sin(\alpha)\cos(\beta)\cos(\theta)} \quad (13)$$

The second laser line orientation k_{yz} in the y,z–plane is predetermined by the laser light section technique given by Eqn. 2 and the associated relation of the laser coordinates y_L and z_L is shown in Eqn. 14.

$$k_{yz} = \frac{y_L}{z_L} = \tan(\varphi) = -\frac{\cos(\alpha)\cos(\beta)\sin(\theta) - \sin(\beta)\cos(\theta)}{\sin(\alpha)\cos(\beta)\sin(\theta)} \quad (14)$$

With Eqns 13 and 14 for the orientation of the laser line it is possible to determine the remaining angles β and θ, shown in Eqns 15 and 16.

$$\beta = -\arctan\left(k_{yx} \frac{\cos(\alpha)\tan(\varphi)+\sin(\alpha)}{\tan(\varphi)}\right) \quad (15)$$

$$\theta = -\arctan\left(\frac{k_{yx}}{\tan(\varphi)}\right) \quad (16)$$

Due to Eqn. 13 the gradient of the laser line k_{yx} in the photograph is dependent on the linear trend of the coil windings represented by θ and the laser rotation around the symmetry axis represented by β. Both angles affect the gradient k_{yx} in the same way and so an estimation using the Eqns 15 and 16 will fail because they can not be determined seperately by a single measurement. The solution to this problem is to make a reference measurement for the skewness of the laser line related to β by using a plane with a defined angle θ instead of the coil front. A vertical plane as reference ($\theta = 0$ °) allows to extract β from Eqn. 13, (see Eqn. 17).

$$\beta = -\arctan\left(k_{yx}(\theta = 0°) \, \sin(\alpha)\right) \quad (17)$$

$$\theta = \arctan\left(k_{yx}\tan(\alpha) + \frac{\tan(\beta)}{\cos(\alpha)}\right) \quad (18)$$

Due the fact that the triangulation angle φ, and so $\alpha \, (= \varphi - \pi/2.)$ is not constant with respect to β, a slight error occurs. Despite the fact that φ is influenced by β, the approximation approach works excellent to determine the laser alignment and the linear trend of the coil front for values of β less than $\pm 15°$. For example a laser rotation by $\beta = -7.5°$ results in an error of θ of less than $0.01°$.

4 LASER LINE EXTRACTION ALGORITHM

Before the coil profil can be determined, the laser line must first be extracted out of the image. Figure 10 shows a steel coil and a laser line projected on it. Due to a rotation of the camera of $90°$ (to obtain the profil length at a higher resolution corresponding to the camera chip with 1392×1040 pixel) the laser line is horizontal in the acquired images. The laser line is clearly visible due to the use of optical filter mentioned in Sec. 1.
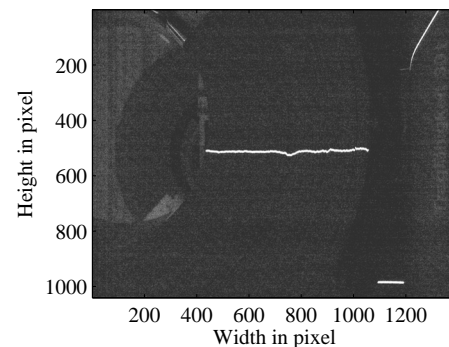
Figure 10: Post–processed image (for better contrast of the laser line) of a steel coil with a laser line.

First of all the algorithm detects if a laser line is present in the image by simply accumulating intensities along rows and searching for a clearly visible maxima. Also a first elimination of packaged coils and a rough estimation of the laser position is done. For coils with packaging material a laser line extraction is meaningless and therefore an early elimination is preferable. After the rough estimation of the laser position, the orignal image is cropped to a vertical region around the laser. Then a median filter with a rectangular mask (with 15×10 pixel) is applied at the cropped image to reduce noise and to smooth the laser line, the result is shown in Fig. 11.

The detection of the maxima positions is an easy way to extract the whole laser line out of the cropped image. But due to the fact that the horizontal position of the coils in the images can vary in dependence on the coil size, the considered image area extends

In: Wagner W., Székely, B. (eds.): ISPRS TC VII Symposium – 100 Years ISPRS, Vienna, Austria, July 5–7, 2010, IAPRS, Vol. XXXVIII, Part 7B

Contents   Author Index   Keyword Index
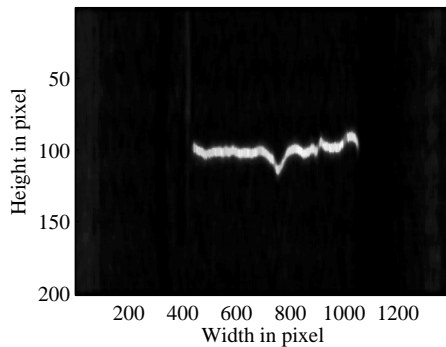
Figure 11: Cropped version of the original image after applying a median filter with differing axes scales.

beyond the coil. So there are also laser lines projected on background geometries present. The background geometries results in sudden steps of the laser line which can lead to a false detections of profile defects. This problem can be reduced by cropping the original image to a vertical region around the estimated laser position. Another problem is the possible presence of edge protection material on the coil that also results in sudden steps of the laser line. Therefore a criterion to only extract reflections of the coil front is needed. The following adaptive algorithm is proposed to extract only valid laser lines:

1. In every row the position of the maximum is detected (under the assumption that only one maximum per column is present, which is referring to the laser) and then saved in the variable $Pos_{Max}(i)$.

2. The maxima positions are normalized to the height of the search region $Pos_{Max}(i) = Pos_{Max}(i) \, / \, Height$.

3. Setting of the start point for the adaptive algorithm in the middle of the laser line to become independent of variing coil sizes.

4. Setting of the start values for the adaptive algorithm with $DevAv(1) = Pos_{Max}(StartPoint)$.

5. Run through the maxima positions left and right of the start point and save positions which satisfy the following criterion $|Pos_{Max}(i + 1) - DevAv(i)| < \sigma$ for $\sigma \leq 1$.

6. If the next maximum position satisfies the criterion from above a new comparison value is calculated for each position with
$DevAv(i + 1) = (DevAv(i) + Pos_{Max}(i + 1))/2$
otherwise the laser line extraction is finished.

Under the assumption (that the alteration of the winding displacements occurs continuously) made in Sec. 1, a restrictive criterion to exclude unvalid steps can be found, see point 5. The local behaviour of the laser line is estimated according to 6 to get an adaptive limitation. The advantages of this algorithm are in its simplicity and speed of operation but still delivers good results. In Fig. 12 the result of the algorithm, the extracted laser line is shown. Alternatively a gray value threshold fiter can be used to extract the laser line but this has the disadvantage that unwanted objects are also included. So it is necessary to use post–processing to adapt the laser line by thinning and to exclude backgroung geometries and edge protection material.

After the laser line is extracted, the overlayed linear trend represented by k_{yx} can be determined by approximating a first–order
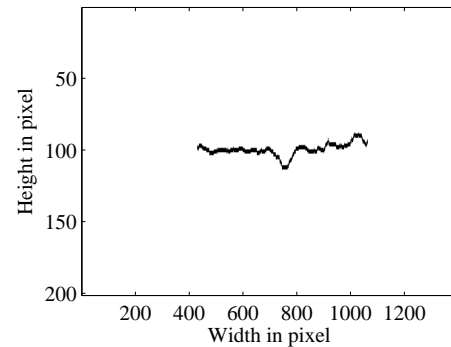
Figure 12: Laser line located on the coil front extracted with an adaptive algorithm out of the cropped image.

polynomial. Subsequently the linear trend of the coil front can be calculated using Eqn. 16. The angle θ is important for quality aspects and also helps to eliminate coils with packaging material, because the packing material results in nontypical values. For example a coil with packaging material is shown in Fig. 13(a) and the extracted laser line with the asymptotic line is shown in Fig. 13(b). In this case θ is $5.7°$ but it should be less than 1 $°$ for unpacked coils.
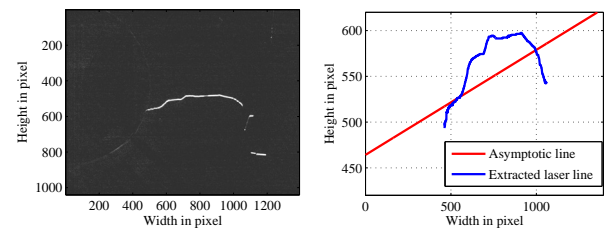
(a) Post–processed image of a coil with packaging material and a laser line.

(b) Extracted laser line (blue) and the corresponding fitted line (red).

Figure 13: Laser line extraction for a coil with packaging material visible.

By using Eqn. 2 the real coil profile can be calculated out of the extracted laser line. For the detection of defects the first derivative of the coil profile is calculated. Then the profile subsegments with a specified raise related to the deviation and height are marked as critical. Additonally critical subsegments in a close neighbourhood are joined. The coil profile and the result for the dection of defects, that are larger than 2 mm, is shown in Fig. 14.
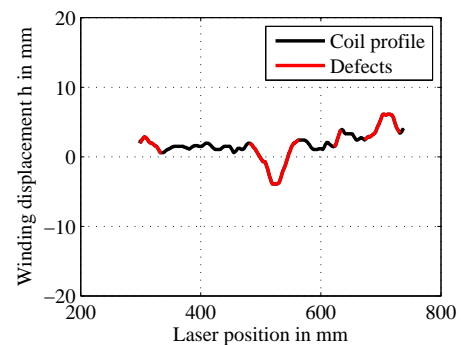
Figure 14: Recognized coil profile (black) and detected defects (red).

5   RESULTS AND DISCUSSION

To evaluate efficiency of the realized measurement system, the maximum systematic error Δh (Schrüfer, 2004) is determined by

In: Wagner W., Székely, B. (eds.): ISPRS TC VII Symposium – 100 Years ISPRS, Vienna, Austria, July 5–7, 2010, IAPRS, Vol. XXXVIII, Part 7B

Contents   Author Index   Keyword Index

Eqn. 19 as a function of the winding displacement h, the triangulation angle φ, the distance Z between camera and coil, and the quantization of the laser position through the camera.

$$\Delta h = \underbrace{\left| \frac{\partial h}{\partial \varphi} \Delta \varphi \right|}_{\substack{\text{error due to} \\ \text{laser align}}} + \underbrace{\left| \frac{\partial h}{\partial Z} \Delta Z \right|}_{\substack{\text{error due to} \\ \text{camera setup}}} + \underbrace{\left| \frac{\partial h}{\partial x} \Delta x \right|}_{\substack{\text{error due to} \\ \text{quantization}}}$$

(19)

Before the total systematic error Δh can be calculated by Eqn. 19, the acquisition of the coil profile must be defined. Therefore Eqn. 2 which describes the calculation of the winding displacement due to the laser light section technique and Eqn. 3 for the mapping properties due the central projection theorem are used. So the final function for h is shown in Eqn. 20.

$$h = \underbrace{\frac{1}{\tan(\varphi)}}_{\substack{\text{laser light} \\ \text{section}}} \underbrace{\left(\frac{Z}{c} + 1 \right) x'}_{\substack{\text{central} \\ \text{projection}}}$$

(20)

$$\Delta h = \left| -\frac{2}{\sin(2\varphi)} \Delta \varphi \right| \cdot |h| + \left| \frac{1}{Z+c} \Delta Z \right| \cdot |h| \\ + \left| \frac{1}{\tan(\varphi)} \left(\frac{Z}{c} + 1 \right) \Delta x' \right|$$

(21)

Equation 21 shows the final result for the systematic error Δh. Considering the specifications for p, c, Z and φ (see Sec. 1) an uncertainly error of $\Delta Z =100$ mm, $\Delta \varphi =2$ ° and $\Delta x' = p$ results in a maximum systematic error Δh of 1.462 mm for a winding displacement h of 5 mm. The main point is that the terms belonging to the camera setup error and the laser alignment error which are scaled by the winding displacement h are smaller than 10^{-1} and the quantization error is a constant 0.487 mm. The systematic error Δh is increasing with nearly $h/10 + 0.487$ mm. Additionally the first term in Eqn. 21 shows that the error due the laser alignment is minimal for triangulation angles φ between $30°$ and $60°$.

In Fig. 15(a) an example for a unpackaged coil with several defects is shown. The final processed coil profile (black), the detected profile defects (red) and the systematic error (green) is shown in Fig. 15(b). It is observable that the calculated coil profile with an insignificantly small systematic error perfectly corresponds to the laser line in the image and the major defects are detected. Futhermore a second example for an unpackaged coil is shown in Fig. 15(c) and processed results in Fig. 15(d). In the second image additional edge protection material is attached to the coil (visible on the left side) but is excluded from the coil profile by the extraction algorithm, as it was demonstrated before.

6 CONCLUSIONS AND FUTURE WORK

We have shown that a recognition of winding displacements for steel coils using the laser light section technique can be realized with a proposed height resolution of less than 1 mm. Furthermore we introduced a mathematical model to eliminate the dependencies from an inaccurate laser alignment and to determine the linear trend of the coil front as another quality aspect. Finally we also have shown that the designed laser line extraction algorithm extracts reliably with sufficient speed the laser line belonging to the coil front. The next step is to improve the pre–process
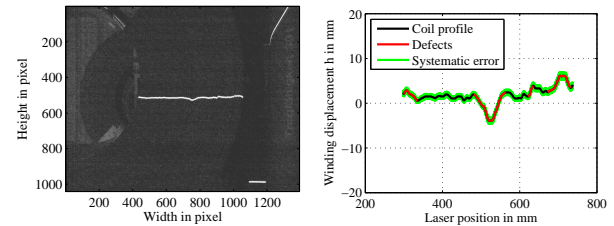
(a) Coil with a laser line and several defects.

(b) Final processed croil profile (black), defects (red) and systematic error (green).

(c) Coil with a laser line and a single defect in the middle.

(d) Final processed croil profile (black), defects (red) and systematic error (green).

Figure 15: Results of the measurement system for two different steel coils.

elimination of steel coils with packaging material and statistically evaluate the defect detection rate of the realized system.

REFERENCES

Cook, M., 2007. Flight Dynamics Principles. Elsevier.

Gonzalez, R. C. and Woods, R. E., 2008. Digital Image Processing. 3 edn, Pearson Prentice Hall.

Horbach, J., 2008. Verfahren zur optischen 3D-Vermessung spiegelnder Oberflächen. Universitätsverlag Karlsruhe.

Kraus, K., 1996. Photogrammmetrie - Band2: Verfeinerte Methoden und Anwendungen. Vol. 2, 3 edn, Ferd. Dümmlers Verlag Bonn.

Luhmann, T., 2003. Nahbereichsphotogrammmetrie — Grundlagen, Methoden und Anwendungen. 2 edn, Wichmann.

Schäfter and Kirchhoff, 2004. Laser Light Section, a Key Feature in 3D Laser Measurement Technique. Schäfter and Kirchhoff.

Schrüfer, E., 2004. Elektrische Messtechnik. 8. edn, Hanser Verlag.

Wu, P., Yu, F., Li, Z., Yan, Z. and Shun, Y., 1993. Analysis technique for the measurement of a three-dimensional object shape. Appl. Opt. 32(5), pp. 737–742.